RESEARCH PAPER

CrossMark

A new thickness parameterization for Discrete Material and Thickness Optimization

J. H. Sjølund[1] · D. Peeters[2] · E. Lund[1]

Abstract

In this work, a new thickness parameterization which allows for internal ply-drops without intermediate voids is introduced in the Discrete Material and Thickness Optimization (DMTO) method. With the original DMTO formulation, material had to be removed from the top in order to prevent non-physical intermediate voids in the structure. The new thickness formulation relies on a relation between density variables and ply-thicknesses rather than constitutive properties. This new formulation allows internal ply-drops which is essential for composite structures as it is common practice to cover dropped plies as to avoid delaminations. Furthermore, it is demonstrated how the new thickness formulation in some cases improves the convergence characteristics. Finally, it is also shown how solid-shell elements can be utilized within the DMTO method for structural optimization of tapered laminated composite structures.

1 Introduction

Variable thickness and use of multiple materials is inevitable for laminated composite structures such as wind turbine blades. Optimization is often essential for design of such structures since multiple conflicting structural criteria in combination with several load cases make it non-trivial to find a good material lay-up. The variable thickness is typically achieved through internal ply-drops. Material selection is not only choosing the best fiber-resin system, possibly in combination with a sandwich core material, but also choosing the best fiber direction for each layer. Typically, the fiber directions are limited to a small prescribed set, for example 0°, ±45°, and 90°, with fixed layer thicknesses. The integer number of plies and finite choices of fiber angles/materials makes it a discrete optimization problem. The optimization problem is further complicated

by manufacturing constraints. Many manufacturing constraints are related to the stacking sequence or thickness change, while others are seemingly obvious, e.g., that adjacent areas of the structure must be inter-connected by continuous plies (often called continuity or blending). A typically required manufacturing constraint for variable thickness structures is regarding the allowable number of ply-drops at a given position, and the distance between subsequent ply-drops. Another common manufacturing constraint is regarding the maximum number of consecutive plies with the same fiber orientation (often called contiguity). An overview of common manufacturing constraints can be found in, e.g., Irisarri et al. (2014) and Peeters and Abdalla (2017). A recent review of optimization approaches for laminated composite structures can be found in Xu et al. (2018).

The perhaps most simple way to parameterize an optimization problem for laminated composite structures is to divide the structure into a number of domains (sometimes called patches), and for each layer in every domain, determine the best material/fiber angle. Evolutionary algorithms (EA) are very popular for optimization of composite structures, as is evident in the recent review by Nikbakt et al. (2018). An advantage of evolutionary algorithms is that they can directly handle discrete variables without relaxation. In a work by Irisarri et al. (2014), an evolutionary algorithm is

---

Responsible Editor: Jose Herskovits

✉ J. H. Sjølund
  jhs@mp.aau.dk

[1] Department of Materials and Production, Aalborg University, Fibigerstraede 16, DK-9220 Aalborg, Denmark

[2] School of Engineering, Bernal Institute, University of Limerick, Limerick, V94 T9PX, Ireland

used to find an optimal composite structure with ply-drops while considering a large number of manufacturing constraints. In another recent example, Albanesi et al. (2018) use a genetic algorithm (GA) for structural optimization of a wind turbine blade where ply start/stop positions along with material choice are the design variables. In general, however, for a large number of design variables, genetic algorithms become computationally demanding.

Another popular strategy are gradient-based "multi-step" methods. Here, the discrete problem is relaxed to a continuous one thereby allowing the use of gradient-based methods. Typically, this is combined with one or more subsequent steps (not necessarily gradient-based) with the purpose of obtaining a manufacturable lay-up. The continuous design variables are usually a combination of laminate thickness and either lamination parameters (Bloomfield et al. 2009; Liu et al. 2011), smeared properties (Zhou et al. 2010; Liu et al. 2011), fiber angles for each ply (Irisarri et al. 2016; Peeters and Abdalla 2016), or ply-group sizing (Sjølund and Lund 2018). Subsequent steps depend much on the targeted manufacturing method and will not be described here.

Gradient-based methods can also be used for solving the discrete problem without subsequent steps. Two similar approaches for simultaneous solution of the optimal thickness and material can be seen in Sørensen and Lund (2013) and Gao et al. (2013). The general idea is here to combine discrete material optimization (DMO) to determine the optimal material for each ply (see Stegmann and Lund (2005)), with topology optimization to determine the optimal thickness distribution. Implicit penalization is used to favor a discrete design. The combined approach is called Discrete Material and Thickness Optimization (DMTO) in Sørensen et al. (2014) where it is also used to minimize the mass of a wind turbine spar. Advances in the method include bi-valued coding to reduce the number of material design variables (see, e.g., Bruyneel (2011) and Gao et al. (2013)), a thickness filter using only one through-the-thickness density design variable per geometry domain (see Sørensen and Lund (2015)), and inclusion of failure criteria constraints (see Lund (2018)). However, due to the topology inspired approach to variable thickness by scaling the constitutive matrix, intermediate voids arise if internal ply-drops are present. So far, this has been solved by only allowing external ply-drops, though it is well known that ply-drops are always covered by outer plies to avoid delaminations.

This work has two objectives. The primary objective is to introduce a new formulation in the DMTO method regarding thickness changes. With the new formulation, internal ply-drops do not create intermediate voids since the density design variables are related to the layer thicknesses instead of layer constitutive properties. This is similar to the parameterization used in Peeters and Abdalla (2016). Furthermore, it will be shown how the new parameterization

influences the sensitivities, in some cases providing better results in fewer iterations. The second objective is to display how solid-shell elements can be utilized in a DMTO setting. Solid-shell elements require a continuous geometry across ply-drops and a simple approach is demonstrated to accomplish this. Benefits of solid-shell elements include access to the full 3D stress state which can be important for strength analysis of ply-drops, and the option of a layer-wise mesh refinement.

The remainder of the article is organized as follows: first the original DMTO method along with the proposed new formulation is presented in Section 2. In Section 3, the optimization approach is described. In Section 4, the new formulation is benchmarked and new capabilities are demonstrated. Finally, the conclusion is given in Section 5.

2 Method

2.1 Discrete Material and Thickness Optimization (DMTO)

In the original Discrete Material and Thickness Optimization method, the parameterization involves the constitutive properties on a layer basis. For each layer, there is a design variable for both the choice of material and regarding if there should be material or not. The choice of candidate material is given by the material design variable vector $\mathbf{x}$ such that

$$x_{plc} = \begin{cases} 1 \text{ if candidate } c \text{ is selected in layer } l \text{ of patch } p \\ 0 \text{ otherwise} \end{cases} \quad (1)$$

while the choice regarding if there should be material or not is given by the density design variable vector $\boldsymbol{\rho}$ such that:

$$\rho_{dl} = \begin{cases} 1 \text{ if there is material in layer } l \text{ of domain } d \\ 0 \text{ otherwise} \end{cases} \quad (2)$$

Here, both domain d and patch p refer to groups of elements. The reason for introducing both is to have individual parameterizations for material and density. The constitutive properties for layer l in element e that is located in geometry domain d and material patch p can be written as

$$\mathbf{E}_{el} = \rho_{dl} \sum_{c=1}^{n^c} x_{plc} \mathbf{E}_c \quad (3)$$

$$\sum_{c=1}^{n^c} x_{plc} = 1 \quad \forall (\rho, l) \quad (4)$$

$$\rho_{dl} \in \{0; 1\} \quad \forall (d, l) \quad (5)$$

$$x_{plc} \in \{0; 1\} \quad \forall (p, l, c) \quad (6)$$

where n^c is the number of candidate materials. In order to use efficient gradient-based optimization methods, the

problem is relaxed, allowing ρ_{dl} and x_{plc} to be intermediate values. Hence, (5) and (6) become

$$\rho_{dl} \in [0; 1] \quad \forall (d, l) \tag{7}$$

$$x_{plc} \in [0; 1] \quad \forall (p, l, c) \tag{8}$$

Since intermediate values of ρ_{dl} and x_{plc} are non-physical, an implicit penalization scheme can be used to favor 0-1 values. If (4) is re-written as

$$\mathbf{E}_{el} = v (\boldsymbol{\rho}) \sum_{c=1}^{n^c} w (\mathbf{x}) \mathbf{E}_c \tag{9}$$

then functions v and w can represent different penalization schemes. Generalizations of two different material interpolation schemes are given by Hvejsel and Lund (2011). The SIMP scheme (solid isotropic material with penalization) corresponds to:

$$v (\boldsymbol{\rho}) = \rho_{dl}^q \tag{10}$$

$$w (\mathbf{x}) = x_{plc}^p \tag{11}$$

where q and p are penalization powers for densities and materials respectively. Similarly, the RAMP scheme (rational approximation of material properties) can be written as

$$v (\boldsymbol{\rho}) = \frac{\rho_{dl}}{1 + q (1 - \rho_{dl})} \tag{12}$$

$$w (\mathbf{x}) = \frac{x_{plc}}{1 + p (1 - x_{plc})} \tag{13}$$

When standard shell finite elements are used, the surface can either refer to the geometric mid-surface of the shell, or it can be offset to bottom or top surface. A change in thickness with the DMTO method is visualized in Fig. 1 when reference is made to the geometric mid-surface. Since only the constitutive properties are affected by a change in $\boldsymbol{\rho}$ the physical laminate thickness is unchanged. Hence even though shell elements with a mid-plane reference is used, the thickness change during optimization occurs in an offset manner.

2.2 New formulation

In the new formulation, it is proposed to remove the relation between $\boldsymbol{\rho}$ and the constitutive properties. Instead the layer thicknesses are functions of densities ρ_{dl} such that a density of one will result in the real ply thickness, a density of zero will result in zero thickness, and intermediate density values will result in intermediate pseudo thicknesses. It is assumed that the candidate materials in layer l patch p have the same ply thickness, t_{pl}. In that case, a pseudo layer thickness
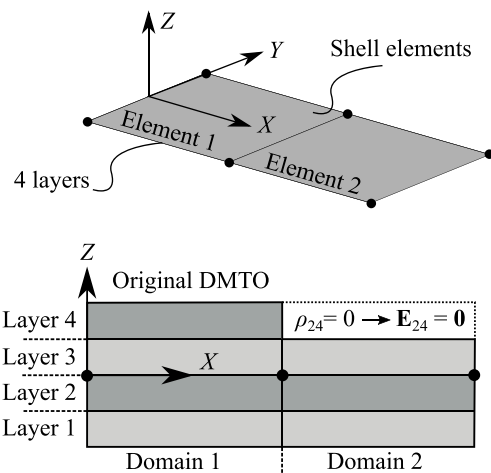

Fig. 1 Visualization of thickness change with the DMTO method, when the geometry refers to the mid-surface. If the density of layer 4 in domain 2 is reduced to zero, the constitutive properties of that layer is likewise reduced to zero. The physical thickness however remains the same

can be calculated as $\tilde{t}_{el} = v (\boldsymbol{\rho}) t_{pl}$. With this relation, the formulation becomes:

$$\mathbf{E}_{el} = \sum_{c=1}^{n^c} w (\mathbf{x}) \mathbf{E}_c \tag{14}$$

$$\tilde{t}_{el} = v (\boldsymbol{\rho}) t_{pl} \tag{15}$$

$$\sum_{c=1}^{n^c} x_{plc} = 1 \quad \forall (\rho, l) \tag{16}$$

$$\rho_{el} \in [0; 1] \quad \forall (e, l) \tag{17}$$

$$x_{plc} \in [0; 1] \quad \forall (p, l, c) \tag{18}$$

A thickness change with the new method is visualized in Fig. 2. Here, it can be seen that if mid-plane reference shell elements are used, then a change in thickness will relocate the layers with respect to the mid-plane such that the resulting new laminate is centered.
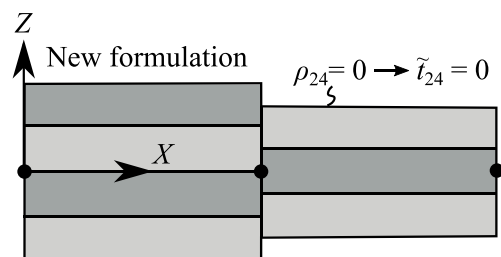

Fig. 2 Visualization of a thickness change using the new formulation, when the geometry refers to the mid-surface. If the density of layer 4 in domain 2 is reduced to zero, the thickness of that layer is reduced to zero. If a mid-plane reference is used, then the layers are moved such that the new thickness-center coincides with the mid-plane

2.3 Offset with dummy layer

Often composite structures are manufactured in a single-sided mold which corresponds to an offset type shell modelling. In this case, the original DMTO method is more appropriate in the sense that the bottom surface is fixed during optimization. In order to enable this behavior for the new formulation, a dummy layer can be added in the top of the laminate (layer $n^l + 1$). This layer has zero or close to zero stiffness similar to a layer with $\rho_{dl} = 0$ in the original DMTO. The thickness of the dummy layer corresponds to the full density thickness of the laminate minus the sum of the current pseudo-thicknesses such that:

$$\tilde{t}_{e(n^l+1)} = \sum_{l=1}^{n^l} \left(t_{pl} - \tilde{t}_{el} \right) \tag{19}$$

The dummy layer offset method is illustrated in Fig. 3.

2.4 Solid-shell approach

Another approach that can deal with offset modelling is solid-shell elements. With solid-shell elements the top and bottom surfaces are explicitly represented by nodes. Furthermore, due to the explicitly defined top and bottom surfaces, the laminate thickness is also explicitly given at each node as the distance between the top and bottom surface nodes. If the solid shell element has varying thickness (described by the 3D volume description), then the layer thicknesses given by the lay-up definition are scaled according to the actual geometric thickness. This is also the usual approach in commercial finite element packages (see, e.g., the SOLSH190 element in ANSYS Inc (2017)). With regard to node positions, if two neighboring elements have different lay-ups, then the coordinates of shared nodes are here taken as the average thickness of the lay-ups. As an example consider a ply-drop across two elements, such that element 1 has a lay-up of $(0°, 0°, 0°, 0°)$ while element 2 has a lay-up of $(0°, 0°, 0°)$. A visualization of the resulting thicknesses can be seen in Fig. 4. When the average thickness is used layers on one side of a shared element edge are stretched and layers on the other side are compressed.
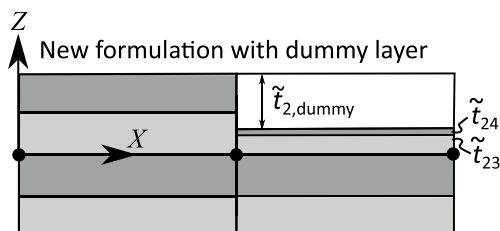

Fig. 3 Visualization of the dummy offset layer combined with the new formulation
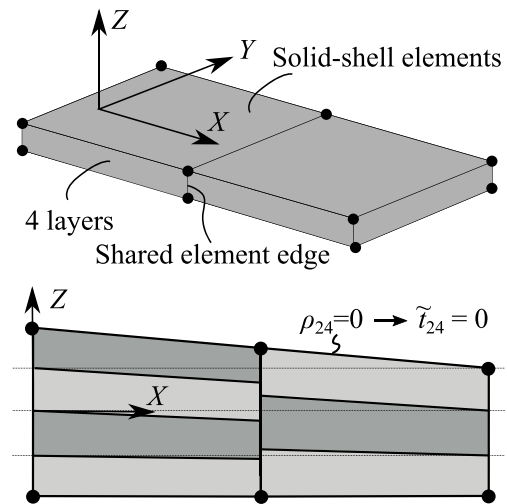

Fig. 4 Visualization of a thickness change using the new formulation combined with solid-shell elements. In this approach intermediate nodes are given the average thickness of neighboring elements. Due to this the layers are stretched/compressed at the interface between elements with different number of layers

2.5 Manufacturing constraints

Manufacturing constraints on thickness variation, maximum consecutive layers and avoiding intermediate voids are given in Sørensen and Lund (2013) but will be repeated here for convenience. The constraint regarding avoiding intermediate voids is particularly interesting as with the new formulation it is not required for the same reasons as in the original DMTO method.

2.5.1 Thickness constraints (avoiding intermediate voids)

With the original DMTO formulation, material must always be removed from the top in order to prevent intermediate voids. In theory, this can simply be formulated by a series of constraints

$$\rho_{d(l+1)} \leq \rho_{dl} \quad \forall d, \quad l = 1, 2, \ldots, n_l - 1 \tag{20}$$

However, Sørensen and Lund (2013) identified that these constraints are not sufficient, and so-called density bands will form through-the-thickness where density variables settle on intermediate values no-matter the penalization. To circumvent this, the limits of the density variables are instead controlled by a series of non-linear constraints. Depending on the density in layer (l), the maximum allowable density in the layer above $(l + 1)$ is:

$$\rho_{d(l+1)} \leq \begin{cases} \frac{T}{1-T}\rho_{dl} & \text{if} \quad \rho_{dl} < (1-T) \\ \frac{1-T}{T}\rho_{dl} + \frac{2T-1}{T} & \text{else} \end{cases} \tag{21}$$
$$\forall d, \quad l = 1, 2, \ldots, n_l - 1, \quad 0 < T \leq 0.5$$

Hence, the maximum value of $\rho_{d(l+1)}$ is a function of ρ_{dl} and T, where T controls the slope of the linear functions

and their intervals. This constraint is visualized in Fig. 5 for different values of the T parameter. For a value of $T = 0.5$ this corresponds to the simple thickness constraint in (20). The essence is that a difference in densities is enforced through thickness. For example for $T = 0.1$ and a density in the first layer of $\rho_{d1} = 0.9$, the next layer is limited to $\rho_{d2} \leq 0.1$. Note that this effect propagates through-the-thickness, i.e., if the density in the second layer has its maximum value of $\rho_{d2} = 0.1$, then the third layer is confined to $\rho_{d3} \leq 0.0111$ etc.

With the new formulation intermediate voids can not appear, and therefore, the thickness constraints are in theory not needed. However, it is still an efficient method to avoid density bands, and will therefore still be used. The major difference is that with the new formulation it is possible to terminate the thickness constraint between, e.g., the second last and the last layer, and thereby covering the ply-drops, without introducing intermediate voids.

2.5.2 Thickness variation

The variation in thickness is the allowed change in thickness from one domain to another. Physically, it corresponds to the maximum number of plies that can be dropped at a given position.

The thickness variation between two elements can be expressed as the difference in the sum of densities. If S is the maximum allowable thickness variation, then the thickness variation constraint between element e and element $e + 1$ can be formulated as

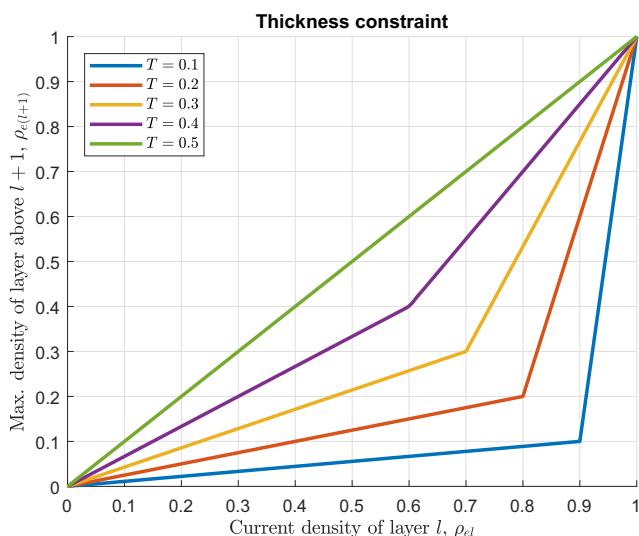$$-S \leq \sum_{l=1}^{n^l} \left(\rho_{el} - \rho_{(e+1)l} \right) \leq S \tag{22}$$

Fig. 5 Plot of the thickness constraint, (21), for multiple values of the T parameter. The maximum allowable density of layer $l + 1$ depends on the density of layer l and the T parameter

2.5.3 Maximum consecutive layers

Another common manufacturing constraint limits the number of consecutive layers of the same fiber angle. If CL denotes the number of maximum consecutive layers, then this constraint can be written for candidate c patch p as

$$\sum_{l=k}^{k+CL} x_{plc} \leq CL, \quad \forall (p, c), \quad k = 1, 2, \ldots, n^l - CL \tag{23}$$

3 Optimization approach

3.1 Optimization problem

The optimization problem can be formulated as

$$
\begin{aligned}
&\min_{\mathbf{x}, \boldsymbol{\rho}} \quad \text{objective} \\
&\text{s.t.} \quad g \leq g_{max} \\
&\qquad \sum_{c=1}^{n^c} x_{plc} = 1 \quad \forall (\rho, l) \\
&\qquad \text{Manufacturing constraints} \\
&\qquad \rho_{el} \in [0; 1] \quad \forall (e, l) \\
&\qquad x_{plc} \in [0; 1] \quad \forall (p, l, c)
\end{aligned}
$$

where $\mathbf{x}$ is the material design variable vector and $\boldsymbol{\rho}$ is the density design variable vector. The objective function and structural constraint g are in this work taken to be compliance and mass respectively (Example 1) or mass and compliance (Example 2 and 3). Manufacturing constraints refer to (21), (22), and (23).

3.2 Sequential linear programming approach

A sequential linear programming (SLP) approach is used to solve the problem. In this approach, in each iteration, the linearized problem is solved based on linear programming. The SLP approach is very robust and has been demonstrated to work well compared to other methods in Sørensen and Lund (2013). Furthermore, the large number of linear constraints resulting from the manufacturing constraints can efficiently be taken into account using modern optimizers. In this work the Sparse Nonlinear OPtimizer (SNOPT) by Gill et al. (2005) has been used for all examples.

In this work, constant move limits of 20% are used in all examples. To have a feasible problem at all times a merit function approach is used (see Sørensen and Lund (2015) for more details). Convergence is defined as a relative change of the merit objective function of less than 10^{-3}. This can be written as

$$\left\| \frac{\Phi^k - \Phi^{k-1}}{\Phi^{k-1}} \right\| < 10^{-3} \tag{24}$$

where Φ denotes the merit function objective and k is the iteration number. Pseudo code for the convergence requirements can be found in Sørensen et al. (2014).

3.3 Continuation approach

Penalization is needed to enforce a 0–1 design. Gradually increasing the penalization during the optimization is used to obtain a strong local optimum. In this work, the penalization factor is increased whenever a design converges with current penalization. In all examples, the generalized RAMP scheme is used with a penalization sequence of

$$p = \{1, 4, 20\} \tag{25}$$
$$q = \{0, 4, 20\} \tag{26}$$

where p is the multi-material penalization and q is the density penalization. For four candidate materials, the RAMP powers 0, 4, and 20 correspond to equivalent SIMP powers of 1, 2, and 3 respectively (see Hvejsel and Lund (2011)).

3.4 Non-discreteness measures

Even though penalization is used, completely discrete results can not be expected. To quantify non-discrete results, measures of non-discreteness for both densities and candidate materials are introduced. The density measure of non-discreteness is inspired by the one used in Sigmund (2007). The basic idea is that if design variables solely consist of 0 or 1, the non-discreteness measure is 0%. If instead all design variables are 0.5 then the measure is 100%. Density non-discreteness (index dnd) is given as

$$M_{dnd} = \frac{4 \sum_{e,l} V_{el} \rho_{el} (1 - \rho_{el})}{\sum_{e,l} V_{el}} 100\% \tag{27}$$

A measure for candidate non-discreteness is given in Sørensen et al. (2014). Here, the basic idea is similar: if all $x_{plc} = \frac{1}{n^c}$ and all $\rho_{el} = 1$, then the measure is 100%. The reason that candidate non-discreteness depends on densities, is that zero density layers should not impact the measure. The candidate non-discreteness (index cnd) is given as

$$M_{cnd} = \frac{\sum_{e,l} V_{el} \rho_{el}^2 \prod_{c=1}^{n^c} \left(\frac{1 - x_{plc}}{1 - \frac{1}{n^c}} \right)^2}{\sum_{e,l} V_{el} \rho_{el}} 100\% \tag{28}$$

3.5 Finite element analysis

Finite element analysis is performed using an in-house research code written in Fortran 95. The code is referred to as the MUltidiciplinary Synthesis Tool (see MUST (2018)).

Results are obtained using both layered standard shell elements and layered solid-shell elements. The used standard shell elements are degenerated 9-node shell elements (see, e.g., Panda and Natarajan (1981)). The solid-shell elements are 8-node elements with 3 degrees of freedom per node. The solid-shell elements utilize enhanced assumed strain (EAS) and assumed natural strain (ANS) to avoid locking phenomena. Details on the solid-shell element formulation is described by Johansen and Lund (2009).

3.6 Design sensitivity analysis

Design sensitivity analysis (DSA) is performed using direct differentiation. The direct differentiation approach is explained in, e.g., Haftka and Gürdal (1992). This is combined with a semi-analytical approach where partial derivatives of the element stiffness matrices are found using central finite-differences. An exception is when design variables are very close to either 0 or 1, then respectively a forward or backward finite difference is used instead. In general perturbations of $z \cdot 10^{-3}$ is used, where z is a generic design variable.

The semi-analytical approach is in general very convenient since the same implementation can be used for multiple elements, however there is a difference between shell and solid-shell elements. With the new formulation, and for standard shell elements, a perturbation of ρ_{dl} corresponds to a perturbation of the thickness of layer l. For solid-shell elements, a change in layer thickness also involves shape optimization since node coordinates must also be changed. This is also shown with examples in Sjølund and Lund (2018).

In this work, the relation between layer thicknesses and node coordinates for solid-shell elements is explicitly coded, such that node coordinates are calculated based on current densities ρ_{dl} whenever the element routine is called. Here, solid-shell elements are only used in an bottom offset manner, meaning that the bottom nodes are always fixed, and a thickness change hence only moves the top nodes. Recalling that the "node-thickness" (distance between nodes belonging to bottom and top surface) is taken as the average thickness of the lay-ups of neighboring elements as shown in Fig. 4, then the coordinate $\mathbf{X}_j$ of a top node j can be calculated as

$$\mathbf{X}_j = \mathbf{X}_i + \bar{\mathbf{n}} \frac{\sum_{e=k}^{n_j^{\text{adj}}} \left(\sum_{l=1}^{n^l} \tilde{t}_{el} \right)}{n_j^{\text{adj}}} \tag{29}$$

where $\mathbf{X}_i$ is the coordinate of the fixed bottom node i, $\bar{\mathbf{n}}$ is the unit vector pointing from $\mathbf{X}_i$ to $\mathbf{X}_j$, and n_j^{adj} is the number of adjacent elements to node j. Hence when

perturbing a density design variable, the node coordinates are also perturbed.

4 Numerical examples and results

The following three examples will demonstrate the new thickness formulation. The original DMTO method is compared to the new formulation with dummy offset, "New (offset)," the new formulation without dummy offset, "New (center)," and the new formulation using solid-shell elements, "New (sol-sh)." Solid-shell models have one element through-the-thickness.

The used material is a glass-fiber reinforced plastic (GFRP) with material properties given in Table 1. These material properties are used in all examples. Four candidate materials corresponding to $[45°, -45°, 0°, 90°]$ are used. Initial candidate design variables are equally distributed such that for four materials the initial material weights for each candidate will be $[0.25, 0.25, 0.25, 0.25]$.

4.1 Example 1

In the first example, the compliance of a cantilever beam is minimized while the mass is constrained to be less than or equal to 3/5 of the full density mass. This benchmark example was also studied in Sørensen and Lund (2013). The cantilever beam consists of five elements, each with five layers, and is shown in Fig. 6a. All elements are linked together in material patches such that a material choice in a given layer is the same across all elements. With regard to the initial density distribution, the first three layers have a density of 1, while the last two layers have a density of 0 such that the starting point is feasible with regard to the mass constraint. The bottom layer is constrained to have full density at all times. Manufacturing constraints include a maximum of one consecutive layer (i.e., no two layers with the same fiber orientation next to each other),

Table 1 GFRP material properties used in all examples

Property	Value	Units
Young's modulus E_{11}	34	GPa
Young's modulus E_{22}	8.2	GPa
Young's modulus E_{33}	8.2	GPa
Shear modulus G_{12}	4.5	GPa
Shear modulus G_{13}	4.5	GPa
Shear modulus G_{23}	4.0	GPa
Density ϱ	1910	kg/m^3
Poisson's ratio ν_{12}	0.29	–
Poisson's ratio ν_{13}	0.26	–
Poisson's ratio ν_{23}	0.26	–

and an allowed thickness variation of one. The thickness constraint given by (21) is included with different values of the T parameter. Results are listed in Table 2, and 3D visualizations are shown in Fig. 6 with layer thicknesses scaled by a factor of 20. Note that the target mass of 3/5 of the full density mass is reached in all cases and hence left out of the table. Candidate non-discreteness, M_{cnd}, reach 0% in all cases and is also left out.
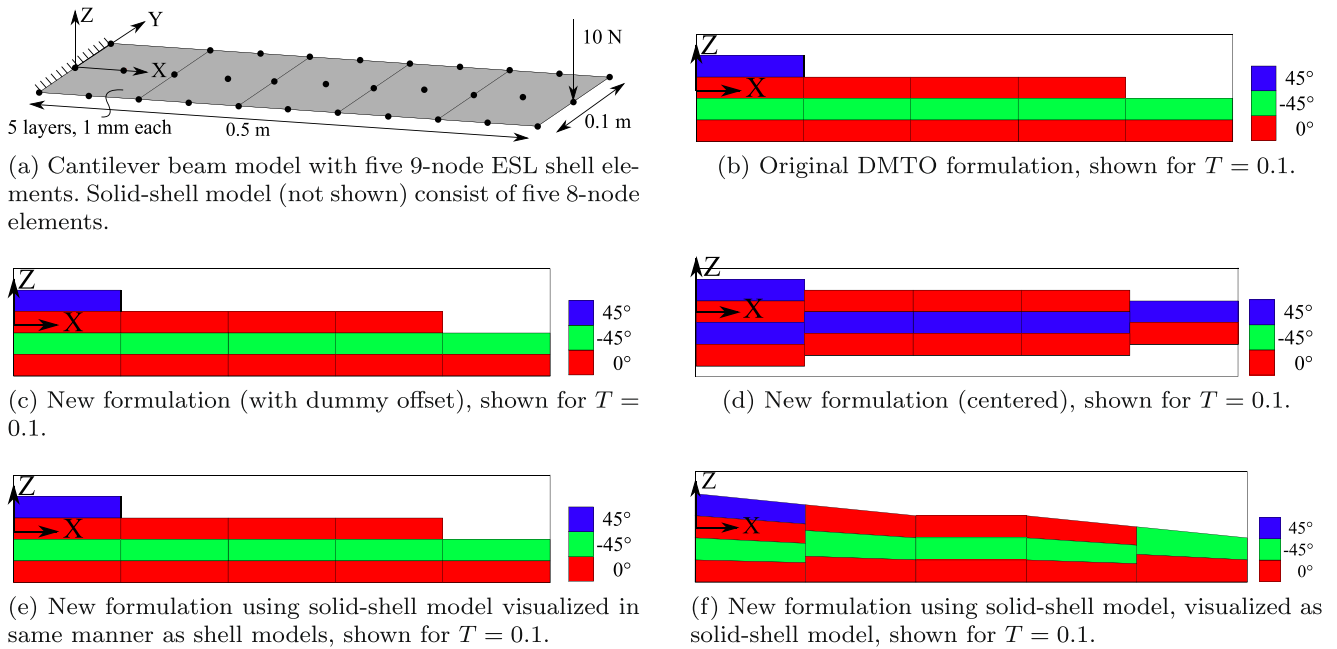
4.1.1 DMTO and new (offset)

The original DMTO formulation and the new formulation (with dummy offset) achieve the same optimum for $T = 0.1$, as can be seen from Table 2 and Fig. 6b, c. The main difference is that the new formulation also finds this optimum for $T = 0.2$ and $T = 0.3$ using less iterations while DMTO results are increasingly non-discrete.

The reason that the original DMTO formulation yields non-discrete results for intermediate T values can partly be explained through the sensitivities as visualized in Fig. 7. For a cantilever beam problem, a change in constitutive properties will have a larger influence on compliance in the top/bottom layers than in the middle layer due to the area moment of inertia. This is also shown in Fig. 7a. Hence, the sensitivities favor adding material to the top and bottom layers, and removing material from the middle. However, at the same time, the thickness constraints enforce that densities of top layers must be less than center layers. These conflicting requirements make the original DMTO method more prone to non-discrete results in this particular example.

With the new formulation, a change in thickness yields the same sensitivity for all layers, as long as each layer has the same material. This is shown in Fig. 7b. This is not initially conflicting with the thickness constraints which in turn helps achieving a discrete optimum. The observation on sensitivities can also explain why $T = 0.4$ in general provides non-discrete results. For example in some cases, in the first element at the constraint, the fourth layer has a density of $\rho_{14} = 0.6$ and the fifth layer $\rho_{15} = 0.4$. The relatively small difference in density, allowed due to $T = 0.4$, makes it such that even though penalization is applied, it does not make up for the fact that the fifth layer is 0° while the fourth is either $\pm45°$.

4.1.2 New (center)

The result for the new formulation (centered) can be seen in Fig. 6d. Since it is true mid-plane reference, the results are not directly comparable with other results. However, for this particular example, the results are very similar to offset results. The found optimum is slightly different than the other results in that both the second and the fourth layer have a fiber angle of $-45°$.

(a) Cantilever beam model with five 9-node ESL shell elements. Solid-shell model (not shown) consist of five 8-node elements.

(b) Original DMTO formulation, shown for $T = 0.1$.

(c) New formulation (with dummy offset), shown for $T = 0.1$.

(d) New formulation (centered), shown for $T = 0.1$.

(e) New formulation using solid-shell model visualized in same manner as shell models, shown for $T = 0.1$.

(f) New formulation using solid-shell model, visualized as solid-shell model, shown for $T = 0.1$.

Fig. 6 Example 1 results for minimization of compliance of a cantilever beam. Results are visualized with layer thicknesses scaled by 20

4.1.3 Solid-shell

The solid-shell optimized design is visualized as the other shell models in Fig. 6e, while the actual computational model with a continuous upper surface is shown in Fig. 6f. The optimum is identical to the one found in the original DMTO and the new formulation (offset). Due to differences between the used standard shell elements and solid-shell elements, results can not be directly compared. However,

Table 2 Example 1 results for minimization of compliance of a cantilever beam with mass constrained to be less or equal to 3/5 of the full density mass

|	$T =$	DMTO	New (offset)	New (center)	New (sol-sh)
Compliance	0.10	4.638e−1	4.638e−1	4.620e−1	4.614e−1
	0.20	4.832e−1	4.638e−1	4.639e−1	4.614e−1
	0.30	5.414e−1	4.638e−1	4.639e−1	4.614e−1
	0.40	8.315e−1	5.485e−1	5.486e−1	6.380e−1
Iterations	0.10	27	17	17	29
	0.20	25	17	17	31
	0.30	30	22	22	29
	0.40	25	28	26	28
M_{dnd}	0.10	0.00%	0.00%	0.00%	0.00%
	0.20	6.32%	0.00%	0.00%	0.00%
	0.30	15.87%	0.00%	0.00%	0.00%
	0.40	36.39%	7.68%	7.68%	15.36%

T refers to the thickness constraint parameter in (21)

the compliances found are very similar to shell model results for the fully converged solutions.

4.1.4 Comparison of models

Comparing the original DMTO formulation to the new formulation with dummy offset, it is clear that the two methods are equivalent modelling wise when comparing the same fully discrete optimum. This can also be seen in Table 2 where the same compliance is obtained for $T = 0.1$. The main difference is in the sensitivities as demonstrated in Fig. 7. The difference in sensitivities is reflected in the different amount of iterations and density non-discreteness at convergence, and in this particular example, the new formulation with dummy offset is favorable.

The new formulation (centered) is the same new formulation but without the dummy offset, meaning that thickness changes during optimization is relative to the mid plane. Hence, when compared to the offset shell models, even the same optimum will not yield the same compliance.

(a) Sensitivities $dC/d\rho_{dl}$ using original DMTO formulation.

(b) Sensitivities $dC/d\rho_{dl}$ using new formulation.
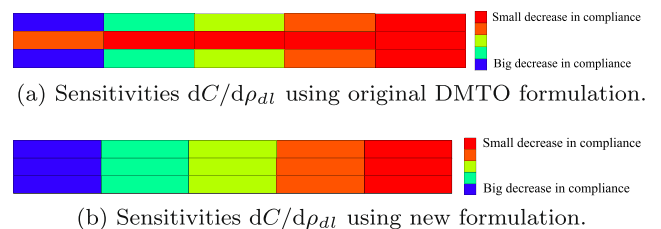
Fig. 7 Comparison of compliance sensitivities with regard to density design variables in 1st iteration where material weights are equal in all layers

However, as expected, the number of iterations and the measure of non-discreteness are very similar to the new formulation with dummy offset.

Results from the new formulation using solid-shell elements are different both due to an entirely different element formulation, but also due to the required continuous geometry across ply-drops. The number of iterations and measure of non-discreteness is also different from the shell models. This difference can be expected since thickness changes here induce skewed element shapes and also involve moving nodes.

4.2 Example 2

In the second example, the mass of a corner-hinged 8 layered plate is minimized while the compliance is constrained to $C \leq 0.9$ J corresponding to approximately 5 full density quasi-isotropic layers. The plate consists of 48x48 elements and is loaded with a nodal force of 40 N in the center. Dimensions are given in Fig. 8a. Density variables are

grouped together in 2×2 element domains. Material patches for each layer span all elements such that in a given layer the same candidate must be chosen for all elements. The initial density distribution is such that the first four layers have full density and the last four layers zero density. The bottom layer is constrained to have full density at all times. Manufacturing constraints include a maximum of one consecutive layer (i.e., no two layers with the same fiber orientation next to each other), and an allowed thickness variation of one. Again, the problem is solved for various T values. Results are listed in Table 3, and in Fig. 8 the best results are visualized with layer thicknesses scaled by a factor of 20. Candidate non-discreteness is 0% in all cases and is not listed in the table.
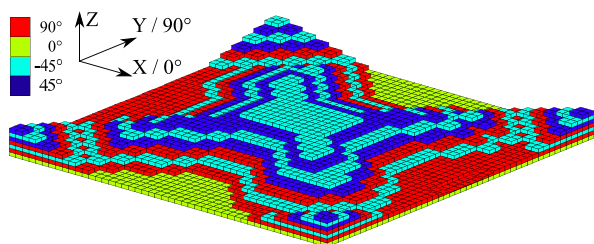
4.2.1 DMTO and new (offset)

The best results for respectively DMTO and New (offset) are shown in Fig. 8b, c. For both the original DMTO and the new formulation (offset), the full density bottom ply is
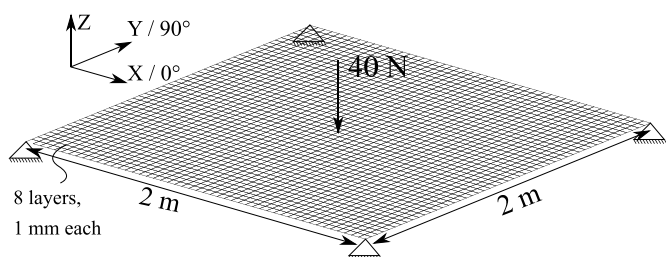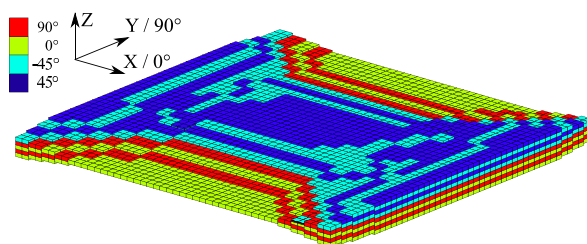

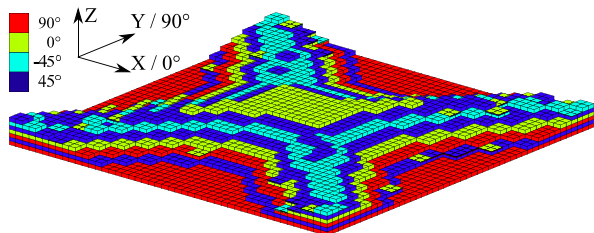(a) The model used for example 2. A corner hinged plate with 8 layers, 24x24 patches, 48x48 elements.
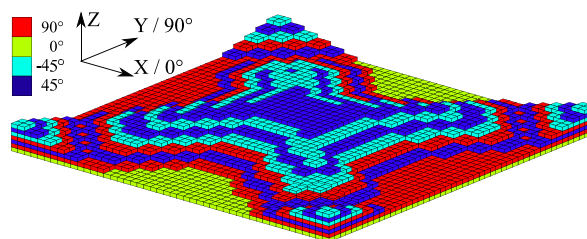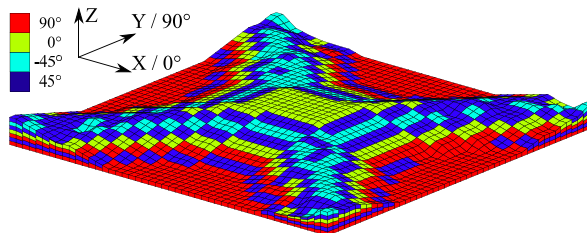

(b) Original DMTO formulation, shown for $T = 0.2$.

(c) New formulation with dummy offset, shown for $T = 0.1$.

(d) New formulation centered, shown for $T = 0.3$.

(e) New formulation using solid-shell model visualized in same manner as shell models, shown for $T = 0.2$.

(f) New formulation using solid-shell model, visualized as solid-shell model, shown for $T = 0.2$.

Fig. 8 Example 2 results for minimization of mass of a corner-hinged plate. Results are visualized with layer thicknesses scaled by 20

Table 3 Example 2 results for minimization of mass of a corner-hinged plate with a constrained compliance, $C \leq 0.9$

	$T =$	DMTO	New (offset)	New (center)	New (sol-sh)
Mass	0.1	30.45	30.32	38.82	32.71
	0.2	30.41	30.33	38.64	30.91
	0.3	30.68	30.36	38.58	31.11
	0.4	32.74	30.94	38.83	31.50
Compliance	0.1	0.900	0.901	0.899	0.901
	0.2	0.900	0.900	0.900	0.900
	0.3	0.900	0.900	0.900	0.900
	0.4	0.900	0.901	0.895	0.900
Iterations	0.1	43	52	88	69
	0.2	51	50	53	42
	0.3	53	45	54	47
	0.4	60	41	52	50
M_{dnd}	0.1	0.20%	0.09%	0.06%	0.52%
	0.2	0.47%	0.14%	0.29%	1.22%
	0.3	5.62%	0.43%	0.21%	3.01%
	0.4	21.73%	6.71%	1.49%	4.96%

chosen to be 0°. This ply directs load in the x-direction to the edges, and the next 90° ply helps redirect the load to the corners; i.e., it balances the 0° ply at the bottom. The remaining layers are dominated by ±45° which in turn lead load to opposing corners. A similar design is reached in the new formulation (offset), although the ordering of the ±45° plies has changed, causing the design to rotate 90°.

For the original DMTO, an increasing non-discreteness can be seen for increasing values of the T parameter. This is not as pronounced for the new formulation (offset). This is similar to what is seen in example 1 and can again be explained from the sensitivities. The number of iterations used show different tendencies. In general, fewer iterations are expected for higher T values since effectively more layers can be changed at once. This is the tendency for the new formulation (offset). However, if the T parameter is too high convergence issues appear which in turn increase the number of iterations. This is the case for the original DMTO method.

4.2.2 New (center)

Results from the new formulation (center) are visibly different from the offset results, as seen in Fig. 8d. Here the first four layers of 0° and 90° plies create a nearly symmetrical base. The upper four plies use ±45° which induce some asymmetry. The main change compared to the other designs is that much more material is placed along two of the edges.

When compared to offset results, the centered formulation particularly impacts areas with one or few layers since these layers will be close to the bending neutral axis and thereby they provide relatively little bending stiffness. This means that a more compliant design can be expected which in turn is reflected on the mass required to obtain a certain stiffness as seen in Table 3. With regard to density non-discreteness and number of iterations, similar tendencies to the new formulation (offset) can be seen, i.e. higher T values yield higher non-discreteness. One exception is seen for $T = 0.3$ which has a lower non-discreteness measure than for $T = 0.2$. Here, it can also be seen that the best found optimum with respect to mass is not always the result with the lowest non-discreteness.

4.2.3 Solid-shell

As in example 1 solid-shell results are visualized both in the manner of the other shell results, see Fig. 8e, and also as an actual solid-shell model with a continuous upper surface, see Fig. 8f. The solid-shell results generally look similar to DMTO/New formulation (offset) results. Non-discreteness is better for low T values, though the lowest T value also yields the highest number of iterations. In this case the best results are obtained for $T = 0.2$.

4.2.4 Comparison of models

Similar results with density placed in a corner-to-corner cross shape are obtained for the methods that are offset during optimization: the original DMTO method, the new formulation with dummy offset, and the new formulation with solid-shell elements. Again, as in example 1, the original DMTO formulation yields more non-discrete results for higher values of the T parameter. This tendency can also be seen for the new formulation in all cases, but is much less pronounced.

Solid-shell convergence is again not directly comparable to shell implementations due to being a different element type, and also here results may be impacted by the induced skewness from thickness changes.

The new formulation centered yields a very different optimum, with density placed in an "H" shape. The different shape is likely due to the modelling difference in which areas with few layers only provide little bending stiffness as they are located near the bending neutral axis. Again low non-discreteness measures are obtained for all T parameters.

4.3 Example 3

The third example demonstrates the capability of the new formulation to have a constant top layer and thereby

covering ply-drops. This is demonstrated on a cantilever beam where mass is minimized while the compliance is constrained to $C \leq 5 \cdot 10^5$ J corresponding approximately to 15 full density layers of 0° plies. The cantilever beam consists of 20 elements with 20 layers and a nodal force of 8000 N is applied at the free end.

In laminated composite structures, it is common to cover the inner and outer surfaces with biaxial ±45° plies. This is both in order to improve the damage tolerance, and to cover ply-drops with a number of continuous plies. Covering ply-drops is needed to avoid delaminations. In this example, both the top and bottom layers are fixed during the optimization, meaning that ply-drops are covered. The fixed layers are achieved by setting the design variable move-limit to 0% for these particular layers. Furthermore, instead of fixing multiple plies in the top and bottom, a ply-thickness of 2 mm is used with equivalent constitutive properties corresponding to a ±45° laminate. The remaining layers 2–19 are 1 mm thick, and can choose between 0°, + 45°, − 45°, and 90° as in the other examples. In order to make the thickness constraint (21) feasible, the top layer is not included in this constraint, i.e., (21) is only defined for $l = 1, 2, \ldots, n_l - 2$. Material patches for each layer span all elements, such that in a given layer the same candidate must be chosen for all elements. The initial density distribution is such that the first 10 layers have full density, the next 9 layers zero density while the last layer also has full density. Manufacturing constraints include a maximum of four consecutive layers, and an allowed thickness variation of one. Again the problem is solved for various T values. Results are listed in Table 4, and in Fig. 9, the best results are visualized with layer thicknesses scaled by a factor of 20. Candidate non-discreteness is 0% in all cases and left out of the table. Original DMTO results are not included in this example as a constant top layer is not possible for a tapered laminate without having intermediate voids.

4.3.1 New (offset)

The best result from the new formulation with dummy offset can be seen in Fig. 9b. All results are dominated by 0° plies as can be expected. Plies of other fiber angles are added due to the rule of a maximum of four consecutive plies and generally ± 45° are preferred in these cases. These plies are generally placed as far towards the middle as can be allowed from the maximum consecutive layer constraint.

When studying the convergence behavior, high values of the T parameter are clearly beneficial with respect to the number of iterations. This makes sense since there are 20 layers and high T values allow density changes in many layers at once, while low values, e.g., $T = 0.1$ effectively

Table 4 Example 3 results for minimization of mass of a cantilever beam with constant top layer with compliance constrained $C \leq 500e3$

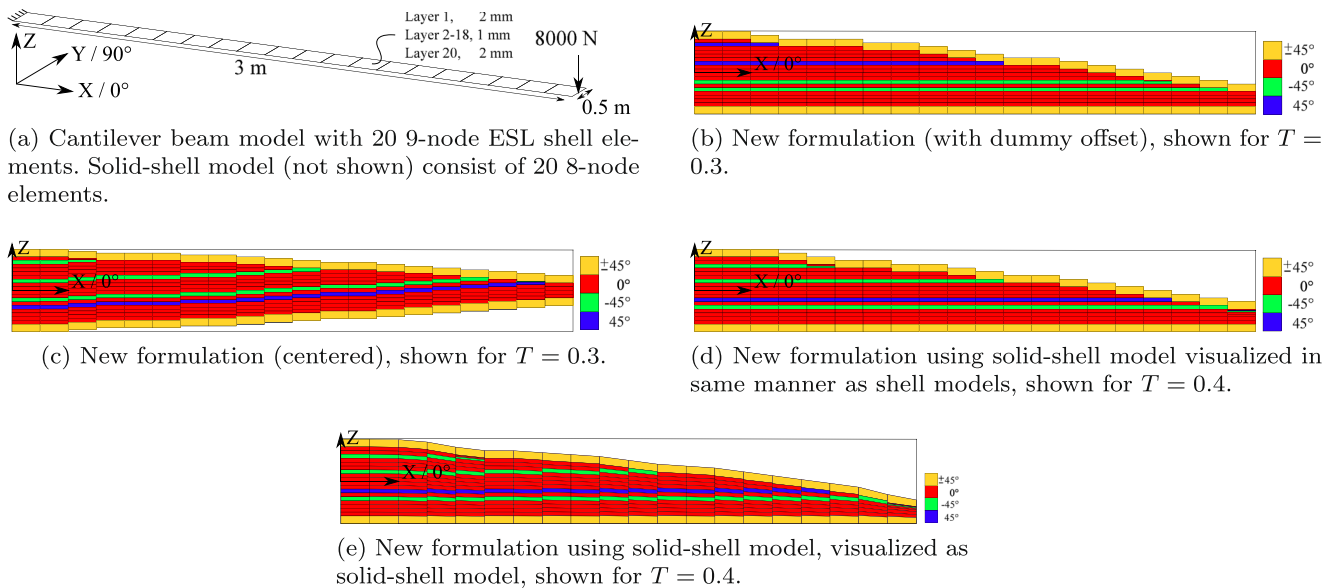|	$T =$	New (offset)	New (center)	New (sol-sh)
Mass	0.1	9.33	9.49	9.52
	0.2	9.20	9.25	9.45
	0.3	9.20	9.19	9.21
	0.4	9.22	9.28	9.20
Compliance	0.1	499.98e3	499.92e3	499.86e3
	0.2	499.98e3	499.97e3	494.90e3
	0.3	499.87e3	499.64e3	500.08e3
	0.4	499.70e3	499.86e3	499.93e3
Iterations	0.1	70	69	52
	0.2	58	56	57
	0.3	49	47	44
	0.4	34	30	30
M_{dnd}	0.1	0.51%	1.25%	0.77%
	0.2	0.77%	1.16%	1.05%
	0.3	0.57%	0.91%	1.22%
	0.4	2.16%	3.07%	1.62%

limits density change to one layer at a time. With regard to density non-discreteness, apart from relative high non-discreteness measures for $T = 0.4$, no clear tendency can be seen from Table 4. It is found from inspection that often the non-discrete layers are placed in the free-end of the beam where the impact of non-discreteness is generally small.

4.3.2 New (center)

The best result obtained for the new formulation (center) can be seen in Fig. 9c. The results are very similar to those obtained in the offset case, and as previously noted, 0° plies are favored with ± 45° being placed as far towards the middle as possible.

4.3.3 New (solid-shell)

The best result obtained for the new formulation (solid-shell) is visualized in the same manner as the shell models in Fig. 9d, and as a solid-shell model with a continuous upper surface in Fig. 9e. Solid-shell results are also very similar to shell results. However, it can be noted that in this case with 20 layers, the solid-shell representation with stretching/compression of layers at a ply-drop boundary looks more realistic than in previous examples. Another observation is that the best result with regard to mass is also the result with the highest non-discreteness measure.

(a) Cantilever beam model with 20 9-node ESL shell elements. Solid-shell model (not shown) consist of 20 8-node elements.

(b) New formulation (with dummy offset), shown for $T = 0.3$.

(c) New formulation (centered), shown for $T = 0.3$.

(d) New formulation using solid-shell model visualized in same manner as shell models, shown for $T = 0.4$.

(e) New formulation using solid-shell model, visualized as solid-shell model, shown for $T = 0.4$.

Fig. 9 Example 3 results for minimization of mass of a cantilever beam with constant top layer. Results are visualized with layer thicknesses scaled by 20

4.3.4 Comparison of models

In this example, a continuous biax layer is enforced as the top layer, and hence ply-drops are covered. With the original DMTO method, this would cause intermediate voids, and hence only the new formulation is used. Similar results are obtained for New (offset), New (center), and New (sol-sh). The results are similar both in terms of the obtained mass, and the density/candidate choices. The density/candidate distribution is intuitive in that 0° plies are favored, and most material is placed towards the constrained end.

5 Conclusion

In this paper, the Discrete Material and Thickness Optimization (DMTO) method has been extended with a new thickness parameterization. The new thickness formulation relates density design variables to layer thicknesses instead of layer constitutive properties. This extension allows internal ply-drops without causing intermediate voids. This is essential since ply-drops should always be covered to avoid delaminations.

The new thickness formulation is compared to the original DMTO method in two examples, and new capabilities are demonstrated in a third example. The DMTO method combined with the new formulation is furthermore demonstrated on solid-shell elements. In many cases, the new thickness formulation shows better convergence properties with more discrete results. Finally, the new formulation is also shown

to be more robust with regard to parameters controlling through-the-thickness density variations.

References

Albanesi A, Bre F, Fachinotti V, Gebhardt C (2018) Simultaneous ply-order, ply-number and ply-drop optimization of laminate wind turbine blades using the inverse finite element method. Compos Struct 184:894–903. https://doi.org/10.1016/J.COMPSTRUCT.2017.10.051

ANSYS Inc (2017) ANSYS 18 mechanical APDL theory reference. Tech. rep., ANSYS, Inc. Canonsburg, Pennsylvania, USA

Bloomfield MW, Herencia JE, Weaver PM (2009) Enhanced two-level optimization of anisotropic laminated composite plates with strength and buckling constraints. Thin-Walled Struct 47(11):1161–1167. https://doi.org/10.1016/J.TWS.2009.04.008

Bruyneel M (2011) SFP—a new parameterization based on shape functions for optimal material selection: application to conventional composite plies. Struct Multidiscip Optim 43(1):17–27. https://doi.org/10.1007/s00158-010-0548-0

Gao T, Zhang WH, Duysinx P (2013) Simultaneous design of structural layout and discrete fiber orientation using bi-value coding

parameterization and volume constraint. Struct Multidiscip Optim 48(6):1075–1088. https://doi.org/10.1007/s00158-013-0948-z

Gill PE, Murray W, Saunders MA (2005) SNOPT: an SQP algorithm for large-scale constrained optimization. SIAM Rev 47(1):99–131. https://doi.org/10.1137/S0036144504446096

Haftka RT, Gürdal Z (1992) Elements of structural optimization. Kluwer Academic Publishers

Hvejsel CF, Lund E (2011) Material interpolation schemes for unified topology and multi-material optimization. Struct Multidiscip Optim 43(6):811–825. https://doi.org/10.1007/s00158-011-0625-z

Irisarri FX, Lasseigne A, Leroy FH, Le Riche R (2014) Optimal design of laminated composite structures with ply drops using stacking sequence tables. Compos Struct 107:559–569. https://doi.org/10.1016/J.COMPSTRUCT.2013.08.030

Irisarri FX, Peeters DM, Abdalla MM (2016) Optimisation of ply drop order in variable stiffness laminates. Compos Struct 152:791–799. https://doi.org/10.1016/J.COMPSTRUCT.2016.05.076

Johansen LS, Lund E (2009) Optimization of laminated composite structures using delamination criteria and hierarchical models. Struct Multidiscip Optim 38(4):357–375. https://doi.org/10.1007/s00158-008-0280-1

Liu D, Toroporov VV, Querin OM, Barton DC (2011) Bilevel optimization of blended composite wing panels. J Aircr 48(1):107–118. https://doi.org/10.2514/1.C000261

Lund E (2018) Discrete Material and Thickness Optimization of laminated composite structures including failure criteria. Struct Multidiscip Optim 57(6):2357–2375. https://doi.org/10.1007/s00158-017-1866-2

MUST (2018) The MUltidisciplinary Synthesis Tool (MUST). Department of Materials and Production, Aalborg University

Nikbakt S, Kamarian S, Shakeri M (2018) A review on optimization of composite structures Part I: laminated composites. Compos Struct 195:158–185. https://doi.org/10.1016/J.COMPSTRUCT.2018.03.063

Panda S, Natarajan R (1981) Analysis of laminated composite shell structures by finite element method. Comput Struct 14(3-4):225–230. https://doi.org/10.1016/0045-7949(81)90008-0

Peeters D, Abdalla MM (2016) Optimization of ply drop locations in variable-stiffness composites. AIAA J 54(5):1760–1768. https://doi.org/10.2514/1.J054369

Peeters D, Abdalla M (2017) Design guidelines in nonconventional composite laminate optimization. J Aircr 54(4):1454–1464. https://doi.org/10.2514/1.C034087

Sigmund O (2007) Morphology-based black and white filters for topology optimization. Struct Multidiscip Optim 33(4-5):401–424. https://doi.org/10.1007/s00158-006-0087-x

Sjølund J, Lund E (2018) Structural gradient based sizing optimization of wind turbine blades with fixed outer geometry. Compos Struct 203:725–739. https://doi.org/10.1016/J.COMPSTRUCT.2018.07.031

Sørensen SN, Lund E (2013) Topology and thickness optimization of laminated composites including manufacturing constraints. Struct Multidiscip Optim 48(2):249–265. https://doi.org/10.1007/s00158-013-0904-y

Sørensen R, Lund E (2015) Thickness filters for gradient based multi-material and thickness optimization of laminated composite structures. Struct Multidiscip Optim 52(2):227–250. https://doi.org/10.1007/s00158-015-1230-3

Sørensen SN, Sørensen R, Lund E (2014) DMTO – a method for Discrete Material and Thickness Optimization of laminated composite structures. Struct Multidiscip Optim 50(1):25–47. https://doi.org/10.1007/s00158-014-1047-5

Stegmann J, Lund E (2005) Discrete material optimization of general composite shell structures. Int J Numer Methods Eng 62(14):2009–2027. https://doi.org/10.1002/nme.1259

Xu Y, Zhu J, Wu Z, Cao Y, Zhao Y, Zhang W (2018) A review on the design of laminated composite structures: constant and variable stiffness design and topology optimization. Adv Compos Hybrid Mater, 1–18. https://doi.org/10.1007/s42114-018-0032-7

Zhou M, Fleury R, Kemp M (2010) Optimization of composite - recent advances and application. In: 13th AIAA/ISSMO multidisciplinary analysis optimization conference